Mechanism of elastic instability in Couette flow of polymer solutions: Experiment

Alexander Groisman and Victor Steinberg
Department of Physics of Complex Systems, Weizmann Institute of Science, 76100 Rehovot, Israel

(Received 8 January 1998; accepted 6 July 1998)

Experiments on flow stability and pattern formation in Couette flow between two cylinders with highly elastic polymer solutions are reported. It is found that the flow instabilities are determined by the elastic Deborah number, De, and the polymer concentration only, while the Reynolds number becomes completely irrelevant. A mechanism of such ''purely elastic'' instability was suggested a few years ago by Larson, Shaqfeh, and Muller [J. Fluid Mech. **218**, 573 (1990)], referred to as LMS. It is based on the Oldroyd-B rheological model and implies a certain functional relation between De at the instability threshold and the polymer contribution to the solution viscosity, η_p/η, that depends on the polymer concentration. The elastic force driving the instability arises when perturbative elongational flow in radial direction is coupled to the strong primary azimuthal shear. This force is provided by the ''hoop stress'' that develops due to stretching of the polymer molecules along the curved streamlines. It is found experimentally that the elastic instability leads to a strongly nonlinear flow transition. Therefore, the linear consideration by LMS is expanded to include finite amplitude velocity perturbations. It is shown that the nature of the elastic force implies major asymmetry between inflow and outflow in finite amplitude secondary flows. This special feature is indeed exhibited by the experimentally observed flow patterns. For one of the flow patterns it is also shown that the suggested elastic force should be quite efficient in driving it, which is important evidence for the validity of the mechanism proposed by LMS. Further, the predicted relation between De and η_p/η is tested. At fixed η_p/η the elastic instability is found to occur at constant Deborah number in a broad range of the solution relaxation times in full agreement with the theoretical prediction. The experimentally found dependence of the Deborah number on η_p/η also agrees with the theoretical prediction rather well if a proper correction for the shear thinning is made. This provides further support to the proposed instability mechanism. © *1998 American Institute of Physics.* [S1070-6631(98)02210-7]

I. INTRODUCTION

Instabilities in flows of polymeric fluids have been attracting increasing attention recently.[1,2] Being interesting by itself, this subject is of major importance for polymer processing and rheometry. Investigation of flow instabilities and pattern formation in polymeric fluids can be considered as a special test of their rheological properties. Hence, it can contribute to our understanding of the polymer fluid rheology. This is also a promising direction in approaching the problem of drag reduction, when minute additions of high molecular weight polymers dramatically reduce turbulent drag.[3]

Polymeric liquids are viscoelastic: The stress field in a polymeric liquid is not uniquely defined by the current rate of strain, but rather depends on the history of the liquid deformations.[4] The polymer molecules are stretched by flow and it takes them some characteristic relaxation time λ to adjust to changes in the flow conditions. One can expect that in polymeric fluids flow instability thresholds and patterns selected above them are different from those in normal Newtonian fluids. This has indeed been found for various types of flows.[5–10] Most of the recent activity, however, is related to the ''purely elastic'' flow instabilities which are observed at very low Reynolds numbers, Re, and do not have their counterparts in Newtonian hydrodynamics.[1,2] These flow instabilities occur in highly elastic polymeric liquids, when large elastic energy stored in the polymer chains stretched by the primary flow is released by a secondary vortex motion.

II. MECHANISM OF ELASTIC INSTABILITY

Most of the purely elastic instabilities that have been reported so far occur in shear flows with curved streamlines.[11–18] This is the flow geometry in which the well-known phenomenon of ''rod climbing'' (Weissenberg effect) is observed.[19,4] If a vertical rotating rod is inserted in a beaker with a highly elastic polymeric liquid, the liquid starts to climb up on it, instead of being pushed outward by the centrifugal force. The reason for this rod climbing is that the rod rotation produces a shear flow, which stretches the polymer molecules around the rod in the azimuthal direction. These elongated molecules act as stretched rubber bands that push the liquid toward the rod (''hoop stress''). In other words, one can say that stretching of the polymer molecules along the streamlines leads to negative normal stress difference $N_1=\tau_{\theta\theta}-\tau_{rr}$, where r, θ, and z are cylindrical coordinates. Since the cylindrical geometry is curvilinear, the nega-

tive normal stress difference produces a volume force, N_1/r, acting inwards in the radial direction that causes the rod climbing.

The Couette–Taylor (CT) system, a simple arrangement of two coaxial cylinders with a working fluid in the annular gap between them, is one of the most well-studied geometries in fluid mechanics.[20] In the usual case the fluid is Newtonian, the outer cylinder is stationary, and the inner cylinder is rotating. If the rotation velocity, Ω, of the inner cylinder is gradually increased, at some critical Reynolds number, Re_c, the basic purely azimuthal Couette flow becomes unstable and a stationary pattern of the Taylor vortex flow (TVF) develops in the system.[20] This Taylor instability is driven by centrifugal force and it has become a paradigm for flow instability and pattern formation in Newtonian fluids. In highly elastic polymeric liquids, where the centrifugal force is totally suppressed by the elastic hoop stress, one can expect a hoop stress driven instability to develop. So, the CT system was the most natural first choice to explore elastic instabilities.

Elastic instability in CT flow was studied both experimentally[11] and theoretically[12] by Larson *et al.* This group of authors and Ref. 12 is referred to below as LMS. They conducted their experiments using dilute solutions of flexible, high molecular weight polymers in viscous Newtonian solvents. Rheological properties of such solutions (Boger fluids[21]) can be described reasonably well by the Oldroyd-B model,[4,1] with the stress tensor given by $\boldsymbol{\tau}=\boldsymbol{\tau}^s+\boldsymbol{\tau}^p$. Here, the contribution $\boldsymbol{\tau}^s=-\eta_s\dot{\boldsymbol{\gamma}}$ is due to Newtonian viscosity of the solvent, η_s; $\dot{\boldsymbol{\gamma}}=\boldsymbol{\nabla}\mathbf{v}+\boldsymbol{\nabla}\mathbf{v}^T$ is the rate-of-strain tensor, and $(\boldsymbol{\nabla}\mathbf{v})^T$ is the transposed tensor of the rate of deformation. (We use the stress sign convention of Ref. 4, so that stress and rate of strain have opposite signs.) The polymer part in the stress is given by

$$\boldsymbol{\tau}^p+\lambda\boldsymbol{\tau}^p_{(1)}=-\eta_p\dot{\boldsymbol{\gamma}}, \tag{1}$$

where λ is the relaxation time and $\boldsymbol{\tau}^p_{(1)}$ is a convected derivative of $\boldsymbol{\tau}^p$:

$$\boldsymbol{\tau}^p_{(1)}\equiv\frac{d\boldsymbol{\tau}^p}{dt}-(\boldsymbol{\nabla}\mathbf{v})^T\cdot\boldsymbol{\tau}^p-\boldsymbol{\tau}^p\cdot\boldsymbol{\nabla}\mathbf{v}. \tag{2}$$

Here $d/dt\equiv(\partial/\partial t+\mathbf{v}\cdot\boldsymbol{\nabla})$ is the usual full time derivative. In a stationary shear flow, $v_x=\dot{\gamma}_{xy}y$, the polymer shear stress is $\tau^p_{xy}=-\eta_p\dot{\gamma}_{xy}$. Thus, an apparent solution viscosity, $\eta=\eta_p+\eta_s$, can be introduced such that $\tau_{xy}=-\eta\dot{\gamma}_{xy}$. The first normal stress difference in such a flow, that is a purely elastic effect, is given by $N_1\equiv\tau_{xx}-\tau_{yy}=-\Psi_1(\dot{\gamma}_{xy})^2$, with the coefficient $\Psi_1=2\eta_p\lambda$. The Oldroyd-B equations can be derived from a microscopic elastic dumbbell model, where a polymer molecule is modeled by two beads connected by a Hookean spring.[4] Then λ is just the relaxation time of a dumbbell, and η_p is proportional to the dumbbell concentration and λ. This always allows one to relate the stress tensor in the Oldroyd-B fluid to average strain and orientation of the dumbbells.

The mechanism of elastic instability in the CT system suggested by LMS is based on the Oldroyd-B model. The primary flow in the CT system with the inner cylinder rotating (Couette flow) is a pure shear flow in the $r\theta$ plane that generates a normal stress difference $N_1\equiv\tau_{\theta\theta}-\tau_{rr}=-2\eta_p\lambda(\dot{\gamma}_{r\theta})^2$ and a radial force N_1/r per unit volume. (This force is counterbalanced by the pressure gradient, $\partial p/\partial r=N_1/r$). A secondary flow in the CT system should include regions of elongational flow in the r direction, where $\partial v_r/\partial r\neq 0$ (see Fig. 1, where TVF is taken as an example of a secondary flow). The simplest form of the deformation rate tensor in coordinates (θ,r,z) is then

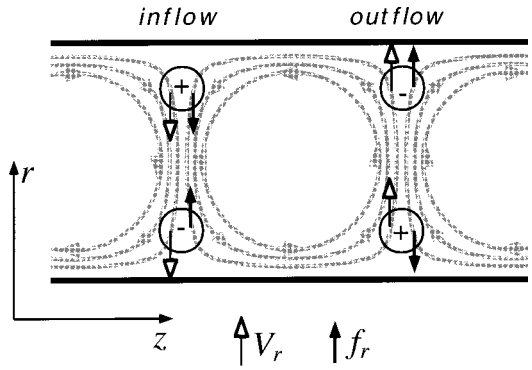

FIG. 1. Schematic drawing of the flow lines, velocities, and elastic forces in $r-z$ cross section of a flow of TVF type in Oldroyd-B fluid. The directions of v_r and f_r are shown by different arrows in four regions (presented by circles) with all possible combinations of signs of v_r and $\partial v_r/\partial r$. The sign of $\partial v_r/\partial r$ is shown by plus and minus signs inside the circles.

$$\boldsymbol{\nabla}_i v_j=\begin{pmatrix}0 & 0 & 0\\ \dot{\gamma}_{r\theta} & \dot{\epsilon} & 0\\ 0 & 0 & -\dot{\epsilon}\end{pmatrix}, \tag{3}$$

where $\dot{\epsilon}\equiv\partial p_r/\partial r$ is a small perturbation.[22] Substituting (3) into Eq. (1), gives the following system of equations for $\boldsymbol{\tau}^p$ (the index "p" is omitted below for simplicity):

$$\tau_{\theta\theta}+\lambda\frac{d\tau_{\theta\theta}}{dt}=2\lambda\dot{\gamma}_{r\theta}\tau_{r\theta}, \tag{4a}$$

$$\tau_{r\theta}+\lambda\frac{d\tau_{r\theta}}{dt}-\lambda\dot{\epsilon}\tau_{r\theta}=-\eta_p\dot{\gamma}_{r\theta}+\lambda\dot{\gamma}_{r\theta}\tau_{rr}, \tag{4b}$$

$$\tau_{rr}+\lambda\frac{d\tau_{rr}}{dt}-2\lambda\dot{\epsilon}\tau_{rr}=-2\eta_p\dot{\epsilon}. \tag{4c}$$

Neglecting the time derivatives and taking $\lambda\dot{\epsilon}\ll 1$, we obtain $\tau_{rr}=-2\eta_p\dot{\epsilon}$, which corresponds to radial stretching of the dumbbells. Being stretched in the radial direction, the dumbbells become more susceptible to the basic shear flow. This is expressed in Eq. (4b) by coupling between τ_{rr} and $\dot{\gamma}_{r\theta}$. (There also exists a direct coupling between $\tau_{r\theta}$ and $\dot{\epsilon}$). As a result, the shear stress increases by $\Delta\tau_{r\theta}=-3\eta_p\dot{\epsilon}\lambda\dot{\gamma}_{r\theta}$, compared to the primary Couette flow. This increased shear stress also couples to $\dot{\gamma}_{r\theta}$ that changes the azimuthal stress by $\Delta\tau_{\theta\theta}=-6\eta_p\dot{\epsilon}(\lambda\dot{\gamma}_{r\theta})^2$. Thus, the addition of the small perturbation of $\partial v_r/\partial r$ to the basic flow generates additional normal stress difference, $\Delta N_1\equiv\Delta\tau_{\theta\theta}-\tau_{rr}=-2\eta_p\dot{\epsilon}[3(\lambda\dot{\gamma}_{r\theta})^2-1]$, and additional elastic volume force in the radial direction, $f_r=\Delta N_1/r$, that can drive the radial flow.

The dimensionless product $\lambda\dot{\gamma}_{r\theta}$ is called the Deborah number, De. It defines the degree of stretching of the polymers by the primary flow. In a CT system with a small gap size, $d \ll R_1$, where R_1 is the inner cylinder radius, $\dot{\gamma}_{r\theta}$ is almost constant across the gap and equal to $\Omega R_1/d$, so that $\mathrm{De} \cong \lambda\Omega R_1/d$. For a small gap and $\mathrm{De} \geqslant 2$, which is usually the case for the elastic instability, the elastic force is given by $f_r \cong -6\eta_p(\partial v_r/\partial r)\mathrm{De}^2/R_1$. (Here the minus is because positive $\partial v_r/\partial r$ generates elastic force directed inwards.) The volume force due to viscous friction, which resists to the radial flow, can be estimated as $\eta(\partial^2 v_r/\partial r^2)$. Since for a vortex flow filling the gap between the cylinders should be $(\partial v_r/\partial r)/(\partial^2 v_r/\partial r^2) \sim d$, the ratio between the elastic driving and the viscous resistance is proportional to

$$K \equiv \frac{\eta_p}{\eta}\frac{d}{R_1}\mathrm{De}^2. \tag{5}$$

The elastic instability should occur when the parameter K exceeds a certain threshold.[23] When the gap ratio, d/R_1, and the polymer contribution to the viscosity, η_p/η, are fixed the elastic instability is expected to arise at constant De independent of λ. If only the gap ratio is fixed, and η_p/η is varied, the Deborah number at the instability threshold should depend on it as $\mathrm{De} \sim (\eta_p/\eta)^{-0.5}$.

The elastic instability mechanism can be shortly formulated as follows.[22] Perturbative radial elongational flow, $\dot{\epsilon}$, couples to the strong azimuthal shear, $\dot{\gamma}_{r\theta}$, that results in a radial volume force, f_r, which reinforces the radial flow. A condition for the reinforcement is that the directions of the force, f_r, and the radial velocity, v_r, coincide, so that $f_r v_r > 0$, and the elastic force makes positive work on the flow. In this relation it is quite instructive to compare the elastic instability mechanism to that of the Taylor instability in Newtonian fluid. The Taylor instability occurs when specific angular momentum of the fluid is decreasing along the radius, which is the case when only the inner cylinder is rotating. Then a fluid element moving outward in the radial direction will find itself surrounded by slower rotating fluid. Thus, this fluid element will experience a centrifugal force larger than its surroundings and will be accelerated outward. A fluid element moving inwards will enter the regions where the fluid rotates faster. Therefore, the local pressure gradient, that exactly counterbalances the centrifugal force experienced by the surrounding fluid, will accelerate this fluid element further inwards. So, in the case of the Taylor instability, the direction of the driving force experienced by a fluid element moving along the radius always coincides with the direction of motion. (There also exists viscous damping that resists the fluid motion.)

The situation is clearly different in the case of the elastic instability described above. Here, the driving force per unit volume, f_r, is proportional to $-\partial v_r/\partial r$ rather than to v_r itself. The effect of the elastic force on flow will be defined by sign of the expression $-v_r(\partial v_r/\partial r) = -\frac{1}{2}\partial(v_r^2)/\partial r$. Situations with all possible combinations of signs of v_r and $\partial v_r/\partial r$ are shown in Fig. 1, where TVF is taken as an example. One can see that the product $f_r v_r \sim -\partial(v_r^2)/\partial r$ is positive near the outer cylinder and negative near the inner cylinder, and should average to zero when integrated over the whole space. Therefore, elastic instability cannot generate a stationary flow of the type shown in Fig. 1.

Up to now we have suggested that the radial velocity is infinitely small, so that the elastic force, f_r, in every point is completely defined by the local velocity gradient, $-\partial v_r/\partial r$. Then, as it can be discerned from Fig. 1, the product $f_r v_r$ averages out to zero when integrated separately over regions where $v_r < 0$ (inflow) or $v_r > 0$ (outflow). The situation changes at finite radial velocity, when the characteristic time of motion of a fluid element across the gap, d/v_r, is of the order of the relaxation time, λ. Since the stress tensor, $\boldsymbol{\tau}^p$, is advected by the fluid motion, the value of the elastic force, $f_r \equiv \Delta(\tau_{\theta\theta} - \tau_{rr})/r$, over the whole inflow becomes influenced by its value in the beginning of the inflow, near the outer cylinder. (The same is true for the outflow.) At the beginning of the inflow f_r is directed inwards. Therefore, the product $f_r v_r$ averaged over the region where $v_r < 0$ should be positive, so that the elastic force should reinforce inflow of a finite amplitude. On the other hand, at the beginning of the outflow (near the inner cylinder) the directions of f_r and v_r are opposite. Thus, by the same token, the average of the product $f_r v_r$ should be negative in the outflow when $d/v_r \simeq \lambda$. In fact, in the Lagrangian coordinates, the finite radial velocity leads to oscillations of $\partial v_r/\partial r$ with a characteristic frequency of v_r/d. These oscillations result in a phase shift between $\partial v_r/\partial r$ and f_r that breaks symmetry between inflow and outflow. So, when v_r is finite, the action of the elastic force in inflow and outflow is not symmetric.

We conclude that, while the elastic instability cannot lead to stationary secondary flow with infinitely small radial velocity, a stationary flow pattern can possibly arise as a result of a finite amplitude transition. Further, one can expect that flow patterns with sufficiently large radial velocity (such that $d/v_r \simeq \lambda$) that are driven by the elastic force, f_r, will exhibit major asymmetry between inflow and outflow.

In the original paper by LMS[12] only linear stability analysis with respect to axisymmetric modes was carried out. It was found that flow mode arising as a result of the elastic instability is oscillatory and appears in a form of a traveling wave moving outward in the radial direction, so that $v_r = Ae^{i(kr-\omega t)}$, where $\omega \simeq 1/\lambda$ and $k \simeq 2\pi/d$. [It is only a general form, since an exact solution should satisfy the boundary conditions, $v_r(R_1) = v_r(R_2) = 0$.] The oscillatory nature of the developing secondary flow was considered by the authors as an inherent part of the elastic instability and was included in their formulation of the instability mechanism. Substituting $\dot{\epsilon} \equiv \partial v_r/\partial r = ikv_r$ into Eq. (4) and taking again $\lambda\dot{\epsilon} \ll 1$, we obtain

$$f_r \cong -\frac{\eta_p\,\mathrm{De}^2}{R_1}\frac{4+2(1-i\omega\lambda)}{(1-i\omega\lambda)^3}ikv_r$$

$$\simeq \frac{2\pi\eta_p\,\mathrm{De}^2}{R_1 d}(2+i)v_r,$$

i.e., the elastic force acts in the direction of the radial velocity and can drive the flow.

The experiments with Boger fluids reported in LMS and in later papers by the same authors[13] indeed revealed elastic

instabilities of oscillatory type, with $\omega \simeq 1/\lambda$, which occurred at vanishing Re. The spatial structure of the observed flow patterns was not resolved, though. Resolution of the spatial structure required more elaborate visualization techniques than were employed in recent experiments by Muller *et al.*[16] A few types of axisymmetric oscillatory patterns were observed in those experiments. The predicted structure of the radial wave of the type $v_r \sim e^{i(kr-\omega t)}$ was not confirmed, though. In fact, the recent, more accurate theoretical studies[15,24] showed that the purely elastic instability in CT flow should always lead to nonaxisymmetric modes. Therefore, it is not quite clear, whether the flow patterns reported in Ref. 16 were really driven by the mechanism suggested by LMS. Recent nonlinear calculations,[24] carried out for the case when both cylinders in a CT system are rotating, imply that the purely elastic instability leads to discontinuous flow transitions (backward bifurcations). So, the nonaxisymmetric modes found in the linear stability analysis[15,24] are supposed to appear as transients only.

One of the main points in experiments on elastic instability in CT flow was to measure the Deborah number, De_c, at the instability threshold and to compare it with the theoretical predictions.[12,13,15,16] However, in spite of considerable efforts, agreement between the experiments and theory remained controversial.

An important prediction of the model described above is that the elastic instability is determined by the nondimensional parameter K. Exploring conditions of the onset of elastic instability in the CT system and the flow patterns appearing above the instability threshold was the main purpose of the experiments that we report in this paper. Verification of the model prediction requires independent variation of η_p/η, d/R_1, and λ. Section III (experiment A) describes experiments at fixed η_p/η and d/R_1, and varying λ. The theoretical prediction of constant De at the instability threshold is confirmed in a broad range of λ. Section IV (experiment B) is devoted to experiments at varying η_p/η. When a correction for the shear thinning of η_p and λ is made, the experimental results are found to be in reasonably good agreement with the theoretical prediction of De $\sim(\eta_p/\eta)^{-0.5}$ at the instability threshold. The results are discussed in the Sec. V.

III. EXPERIMENT A

A. Experimental apparatus and techniques

In this section we report results of our experiments on CT flow in a 300 ppm solution of high molecular weight PAAm [polyacrylamide, $M_w=(4-6)\times 10^6$, with a broad molecular weight distribution]. The Newtonian solvent was a viscous sugar syrup, a 63% solution of saccharose in water. Molecules of PAAm are flexible and its solutions exhibit significant first normal stress difference in shear flows,[21] in agreement with the Oldroyd-B model. Viscoelastic properties of the PAAm solution were studied in the regimes of constant and oscillating shear rate using Haake 100 viscometric system. The temperature of the liquid was controlled up to 0.05 °C, which corresponded to variation of η_s by less than 0.5%. The apparent solution viscosity, $\eta(\dot\gamma)\equiv\tau/\dot\gamma$, was measured with a precision of about 1% in range of $\dot\gamma$ from 0.1 to 6 s^{-1}. The polymer part of viscosity, $\eta_p(\dot\gamma)\equiv\eta(\dot\gamma)-\eta_s$, exhibited significant shear thinning (η_p at $\lambda\dot\gamma=4$ was lower by 25% than at $\dot\gamma\to 0$, see Fig. 2 below). So, to avoid ambiguity, the values of $\eta_p(\dot\gamma)$ and $\eta(\dot\gamma)$ at $\dot\gamma\to 0$, denoted below as η_p^0 and η^0, respectively, are taken as representatives. The shear thinned values of $\eta_p(\dot\gamma)$ and $\eta(\dot\gamma)$ are denoted by η_p^+ and η^+, respectively.

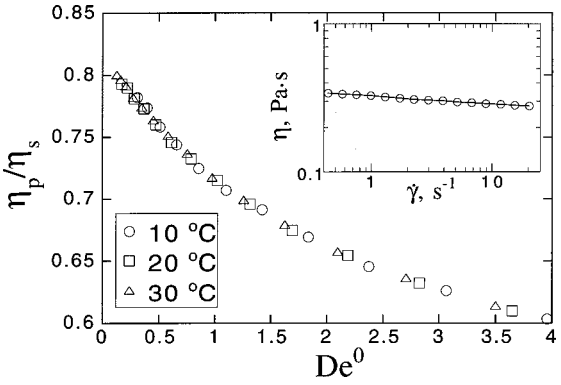

FIG. 2. Relative polymer viscosity, $\eta_p/\eta_s\equiv(\eta(\dot\gamma)-\eta_s)/\eta_s$, as a function of the Deborah number, $\mathrm{De}^0=\lambda^0\dot\gamma$, at three different temperatures. The values of η_p/η_s plotted for 10, 20, and 30 °C are the measured values multiplied by factors of 0.977, 0.986, and 1, respectively. Inset: viscosity at 10 °C as a function of the shear rate.

Carrying out rheometric measurements in the oscillatory regime, we obtained the values of shear stress amplitude, τ_0, and the phase shift, δ, between the stress and the shear rate, $\dot\gamma$, as functions of the oscillation frequency, ω, and the shear rate amplitude, $\dot\gamma_0$. The phase shift, $\delta_p(\omega,\dot\gamma_0)$, between the oscillations of the polymer part of stress, τ^p, and $\dot\gamma$ was calculated then as $\delta_p=\tan^{-1}[\tau_0\tan(\delta)/(\tau_0-\tau_0^s)]$, where τ_0^s is the stress amplitude measured with the pure solvent. The relaxation time, $\lambda(\dot\gamma_0)$, taken as $\delta_p(\omega,\dot\gamma_0)/\omega$ at $\omega\to 0$, was a decreasing function of $\dot\gamma_0$. This shear thinning of the relaxation time was rather strong, so that $\lambda(\dot\gamma_0)$ measured at $\dot\gamma_0=0.5/\lambda$ was smaller by 30% than $\lambda(\dot\gamma_0)$ at $\dot\gamma_0\to 0$. Therefore, the value of $\lambda(\dot\gamma_0)$ at $\dot\gamma_0\to 0$, denoted below as λ^0, was used as a representative relaxation time. It could be determined with an error of about 10%, that was mostly due to two extrapolations to zero. The Deborah number based on λ^0 is designated as De^0, $\mathrm{De}^0=\lambda^0\dot\gamma$. (Note that in our previous publications[9,18,25] $\lambda^0\dot\gamma$ was designated as De.) The shear thinned relaxation time, $\lambda(\dot\gamma_0)$, is denoted in the text as λ'.

The experiments were carried out in a temperature controlled CT system with the cylinder radii $R_1=34$ mm, $R_2=41$ mm, and the length $L=516$ mm. The gap ratio, d/R_1, was 0.206. The gap ratio is not very small, yet this is not supposed to influence the functional dependence of K on λ and η_p/η_s. In the explored temperature region of 5–30 °C the solvent viscosity, η_s, changed from 0.29 to 0.052 Pa s. On the other hand, the ratio $\eta_p(\dot\gamma)/\eta_s$ almost did not depend on temperature, as long as the Deborah number, $\lambda^0\dot\gamma$, was kept constant. Dependencies of η_p/η_s on De^0 at three different temperatures are shown in Fig. 2. One can see that the dependencies of η_p/η_s on the Deborah number at 10, 20, and 30 °C collapse onto a universal curve, when the func-

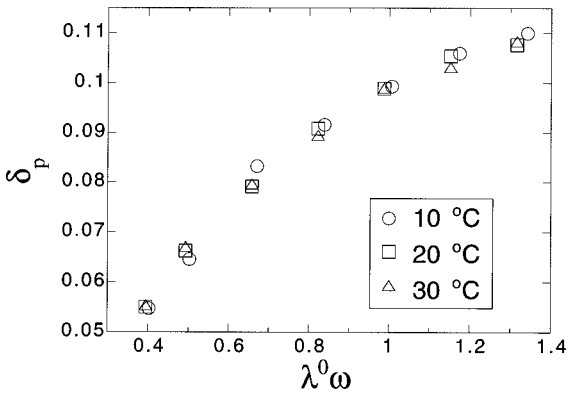

FIG. 3. The phase shift, δ_p, between the oscillations of the polymer part of stress, τ_p, and the shear rate, $\dot{\gamma}$, as a function of the oscillation frequency, ω, multiplied by λ^0. The phase shift was measured at 10, 20 and 30 °C at a constant normalized shear rate amplitude, $\lambda^0\dot{\gamma}_0=1.2$.

tions $\eta_p(\mathrm{De}^0)/\eta_s$ are multiplied by factors of 0.977, 0.986 and 1, respectively. So, η_p^0/η_s has an almost constant value of about 0.83 in the whole experimental range, and shear thinning of η_p depends on the Deborah number only.

The relaxation time, λ^0, was carefully measured according to the procedure described above at one temperature that was used as a reference point. Then the dependencies of δ_p on ω at different temperatures were measured with the shear rate amplitudes, $\dot{\gamma}_0$, chosen inversely proportional to the expected values of λ^0. In this way the proper values of λ^0 were found, such that dependencies of δ_p on $\lambda^0\omega$ measured at constant $\lambda^0\dot{\gamma}_0$ collapsed onto a universal curve that is shown in Fig. 3. By this procedure the ratios between the relaxation times, λ^0, could be determined with precision of about 2%, which defined the relative error of our estimates of De^0 at different temperatures. It was found that the relaxation time approximately followed the relation $\lambda^0 \sim \eta_s/T^2$. So by changing the temperature in the CT column from 30 to 5 °C we changed λ^0 from 0.43 to 3.1 s.

At the conditions of fixed d/R_1 and η_p/η realized in the CT flow, the onset of the elastic instability should be defined by the Deborah number, while the inertial Taylor instability is expected to occur at certain value of Re. Therefore, an appropriate nondimensional parameter, κ, that defines the relation of the elastic and inertial effects is the ratio $\mathrm{De}^0/\mathrm{Re}$ ($\mathrm{Re}=\Omega R_1 d\rho/\eta^0$). The parameter κ does not depend on the cylinder rotation and is also equal to the ratio of λ^0 to the viscous diffusion time, $\kappa=\lambda^0/t_{\mathrm{vd}}$. The viscous diffusion time, $t_{\mathrm{vd}}\equiv d^2\rho/\eta^0$, where ρ is density of the liquid, is a characteristic time of velocity fluctuation decay due to viscous friction. In the limit of small κ the elastic effects disappear, while the case of large κ corresponds to the purely elastic instability. In the explored region of temperatures κ varied from 0.78 to 26.6.

The critical Reynolds number found at the onset of the Taylor instability in Newtonian fluids in our CT column was $\mathrm{Re}_c=88$. It was predicted in Ref. 15 that for $d/R_1=0.13$ and $\eta_p/\eta=0.20$ the Deborah number, De_c, at the elastic instability threshold should be about 15. Assuming that K is constant at the instability threshold, we obtained for our d/R_1 and η_p/η the critical Deborah number $\mathrm{De}_c=8$. The largest value of Re at the elastic instability threshold (it corresponds to the smallest κ, since $\mathrm{Re}=\mathrm{De}^0/\kappa$) was expected to be about 10, which is much lower than Re_c. Therefore, the elastic effects were expected to dominate in the whole experimental range.

The flow in the CT column was visualized by three different methods. Adding to the polymer solution a moderate amount of light reflecting flakes (0.6% of the Kalliroscope liquid) we observed the flow in the ambient illumination. In order to explore the flow structure across the gap in the $r-z$ cross section, we used the light sheet technique. A small amount (0.15%) of the reflecting flakes was added to the polymer solution and a laser beam expanded by a cylindrical lens to a sheet of light parallel to the column axis was used for illumination. Flow patterns were captured and digitized with the aid of a charge-coupled device (CCD) camera and a frame grabber. By plotting darkness profiles of the flow patterns along a fixed line in consecutive moments of time we obtained space–time diagrams of the flow. In other experiments, the laser Doppler velocimetry (LDV) technique was used for local velocity measurements.

B. Results

The purpose of the experiments reported in this section was to study the dependence of the flow stability on κ and De at constant η_p/η, and to explore flow patterns above the instability threshold. The sequence of flow patterns in the CT column was the same in the whole studied region of κ. The observed patterns can be divided into two branches.

The patterns belonging to the first branch were characterized by very low secondary velocities ($v_r \ll d/\lambda$) and very long evolution times. The flow patterns could evolve and transform for tens of minutes and even hours at fixed cylinder rotation velocity, Ω. So, it was very difficult to find the critical Deborah number, De^0 (we could estimate it as being below 12). Some of the flow patterns from the first branch were similar to those reported in Ref. 16, where low secondary velocities and long evolution times were also noted. As it has been found recently,[26] Boger fluids subjected to long shear flows of $\mathrm{De}\simeq 1$ can undergo subtle changes that are beyond the scope of any simple rheological models. Thus, it is not clear, whether the slowly developing flow patterns from the first branch are related to the instability mechanism by LMS, and whether they can be described by a rheological model of the Oldroyd-B type. Therefore, we concentrated on the second branch of flow patterns that had characteristic velocities, frequencies, and evolution times scaling with λ.[18,25] These flow patterns that exhibit strong vortex motion are the main subject of the present paper. Nevertheless, before we start to discuss them, we would like to present one particular flow pattern from the first branch.

Space–time diagrams of this axisymmetric pattern, that we called radial wave, RW, are shown in Figs. 4 and 5. The pattern was observed at $\mathrm{De}^0=18$ and $\mathrm{Re}=0.03\,\mathrm{Re}_c$, so that inertial effects were very small. The diagrams in both Figs. 4 and 5 are plotted using the light sheet visualization technique. The spatial coordinate in Fig. 4 is taken along a line parallel to the column axis, near the middle of the gap.

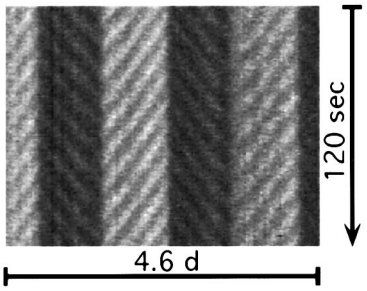

FIG. 4. Space–time plot of RW with the space coordinate taken along a line parallel to the column axis at the middle of the gap. The flow was visualized by the light sheet technique.

(Similar space–time diagrams were reported in Ref. 16.) The diagonal lines in Fig. 4 correspond to traveling waves propagating along the column axis. Domains of the waves propagating to the right and to the left are separated by sources and sinks that appear in Fig. 4 as vertical lines. (Three sources and two sinks can be seen in Fig. 4). The distance between the sources and the sinks is about $0.94d$ in average, so that the space between the cylinders is divided into cells which are almost square in the $r-z$ cross section. In Fig. 5 the spatial coordinate is taken in the radial direction, the axial position being in the middle between a source and a sink. One can see waves traveling radially inwards. In can be discerned from Figs. 4 and 5 that the components of the wave vector $\vec{k}(k_z,k_r)$ are both equal to about $3\pi/d$. Thus, the waves seen in Figs. 4 and 5 are due to vortices that move diagonally inwards inside the square cells built by sources and sinks. Since $|\vec{k}|\approx 4.5\pi/d$, there should be 4–5 vortices simultaneously moving inside a cell. The structure of RW seems to agree with the radially traveling waves predicted in Refs. 12 and 13. On the other hand, characteristic frequency, ω, of RW is about $0.4/\lambda^0$ (and about $0.1/\lambda'$), which is significantly lower than the theoretical prediction.[12,13] More important, the radial waves always moved inward (Fig. 5) in contrast to the outward propagating waves considered in Refs. 12 and 13).

The transition to the second branch of patterns occurred if the Deborah number was increased up to 20–25. As a result of it, strong chaotically oscillating vortices that we call disordered oscillations, DO,[9,18] appeared in the column, Fig. 6(a). The transition was abrupt and strongly hysteretic,

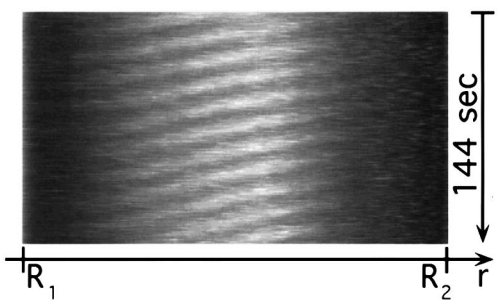

FIG. 5. Space–time plot of RW with the space coordinate taken along the column radius (light sheet visualization). One can see waves traveling in radial direction inwards.

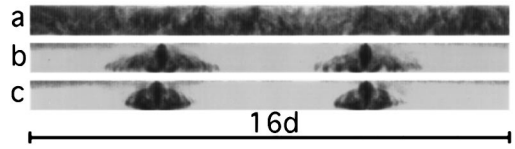

FIG. 6. Various flow patterns that are observed as Ω decreases from Ω_0—the rotation velocity of the DO onset, to $0.47\Omega_0$—the velocity of the diwhirl decay. The flow was visualized by the light sheet technique. The top and the bottom of each strip correspond to the outer and the inner cylinder, respectively. (a) $\Omega=\Omega_0$, disordered oscillations; (b) $\Omega=0.59\Omega_0$, oscillatory strips; (c) $\Omega=0.48\Omega_0$, stationary diwhirls.

which agrees with the recent theoretical prediction.[24] If Ω was lowered afterwards, DO decayed to separate oscillating strips with a core in the middle, Fig. 6(b). As the rotation velocity was decreased further, these oscillatory strips became stationary vortex structures, Fig. 6(c), coined by us as solitary vortex pairs or ''diwhirls.'' [18] The diwhirls decayed and the Couette flow was finally recovered at a rotation velocity that could be as low as 45% of that at the DO onset.

A space–time diagram of the transition to DO is shown in Fig. 7. The cylinder rotation velocity was abruptly raised from zero to a few percent above the critical value, so that the transition to DO occurred quickly and slow patterns belonging to the first branch did not have time to develop. One can see that DO arise from a transient oscillatory mode with continuously growing amplitude that appears as a result of instability of the Couette flow. The frequency of the oscillations at large κ is inversely proportional to the relaxation time ($\omega\simeq 1/(2\lambda^0)$),[25] which is evidence for the elastic nature of the transient mode. This mode is nonaxisymmetric. It appears as a spiral traveling along the axis of the column or a superposition of two spirals traveling in opposite directions that results in a standing wave with azimuthal wave number $m=1$ (rotating standing wave, RSW[9]). This spatial structure agrees with the recent predictions for the elastic instability.[15] The axial wave number of the transient mode at high κ was about 4.3,[25] which is also quite close to the prediction of Ref. 15. The same kind of transient mode, neutral linear oscillations, NLO in Ref. 9, was observed earlier at lower κ, where elastic and inertial effects were quite comparable. The oscillation frequency of NLO at low κ was proportional to $1/t_{\mathrm{vd}}$

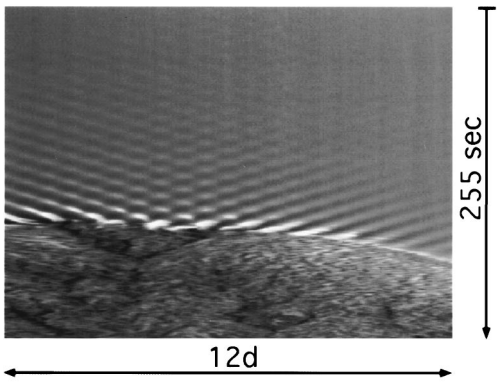

FIG. 7. Space–time plot of transition from the Couette flow to DO with the space coordinate taken along the column axis (ambient illumination). One can see patches of traveling and standing waves that appear as transients.

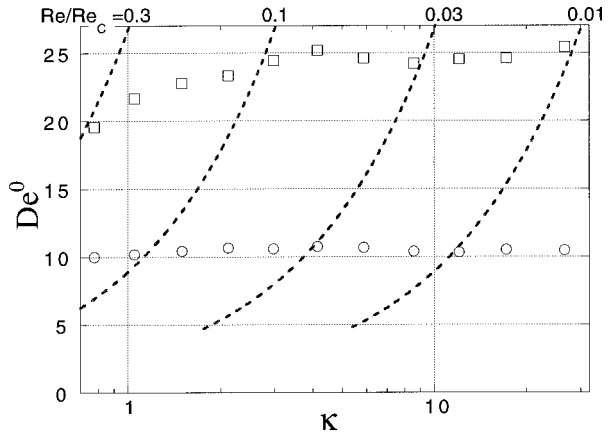

FIG. 8. Dependence of De^0 at the DO onset (squares) and the diwhirl decay (circles) on the elasticity parameter κ. The dashed lines correspond to different constant values of Re/Re_c, from 0.01 to 0.3.

rather than to $1/\lambda^0$. Therefore, the neutral transient traveling spirals and RSW can obviously be driven by both elastic and inertial forces, and in this way connect the regions of low and high elasticity.[25]

The Deborah numbers at the onset of DO and at the decay of the diwhirls are plotted in Fig. 8 as functions of κ. One can see that in the whole experimental region, $\lambda^0 = 0.43-3.1$ s, the decay of the diwhirls occurs at a constant Deborah number, $De^0=10.5$. At large κ, the Deborah number of the DO onset also becomes a constant, $De^0=25$, while the Reynolds number becomes completely irrelevant. This proves that both DO and the diwhirls are driven by elastic stresses. A constant value of De^0 at fixed η_p^0/η^0 and d/R_1, and varying λ^0 is in full agreement with the predictions of LMS for the elastic instability threshold. We notice, however, that the value of 25 found for De^0 at the DO onset is significantly higher than expected $De_c=8$. This large discrepancy can be connected to the shear thinning of λ that is discussed in more details in Sec. IV.

Stationarity of the diwhirls [Fig. 6(c)] gave us the possibility of an accurate study of the flow structure by LDV. The dependence of v_r in a diwhirl on the axial position, z, is presented in Fig. 9. A schematic drawing of the flow lines in a diwhirl is shown in Fig. 10. [It is made on the basis of Fig. 6(c), Fig. 9 and other LDV measurements.[18]] One can see

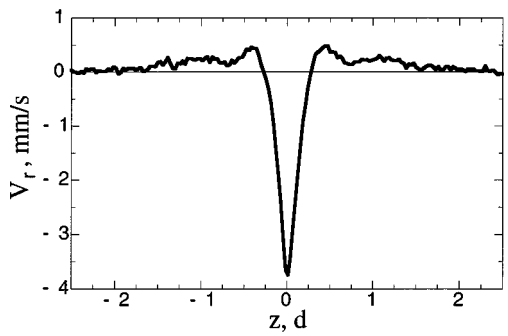

FIG. 9. Radial component of the fluid velocity v_r in a diwhirl, measured by LDV at a constant radius (near the middle of the gap, where v_r is maximal), as a function of position along the column axis, z.

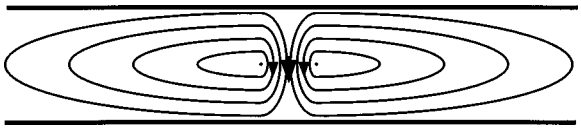

FIG. 10. Schematic drawing of the flow lines in a diwhirl.

that a diwhirl is indeed a pair of vortices. There is a striking asymmetry between the inflow and the outflow. The intensive inflow is concentrated in the narrow core of the pair (that corresponds to the dark spindle-shaped cores in Fig. 6), while the outflow is slow and spreads over the wide edges of the diwhirl. The asymmetry of the distribution of v_r agrees well with the asymmetric response of the elastic forces to inflow and outflow discussed above. This is additional strong evidence that the diwhirls are driven by the elastic hoop stress.

The elastic forces driving the flow in the diwhirls can be understood more clearly from the following arguments. The maximal values of the radial velocity, $v_{r,\max}$, measured in the centers of the diwhirls at their decay were about $0.5d/\lambda^0$ (and larger at higher De^0).[25] For substitution into Eq. (4) it is more proper (it is discussed in more detail in Sec. IV) to use the shear thinned value of the relaxation time, λ'. At the diwhirl decay it was $\lambda' \cong 0.2\lambda^0$, so that $\lambda' v_{r,\max}/d \cong 0.1$. This relation has two important implications. First, the time derivatives in Eq. (4) cannot be neglected now. Since the signs of $\partial v_r/\partial r$ near the inner and the outer cylinder are always opposite (for both the inflow and the outflow, Fig. 10), we expect the perturbations in stress, $\Delta\boldsymbol{\tau}$, there to be opposite as well. Therefore, in the core of a diwhirl $\lambda'(d\boldsymbol{\tau}/dt) \cong \lambda' v_r(\partial\Delta\boldsymbol{\tau}/\partial r) \cong 2\lambda' v_{r,\max}\Delta\boldsymbol{\tau}/d \cong \Delta\boldsymbol{\tau}/5$ is of the same order as $\Delta\boldsymbol{\tau}$ itself. (The partial time derivative, $\partial\boldsymbol{\tau}/\partial t$, is identically zero.) That is, although in the laboratory frame the flow in a diwhirl appears as stationary a moving fluid element will experience variations of $\partial v_r/\partial r$ and $\Delta\boldsymbol{\tau}$ on a time scale of d/v_r that is close to the relaxation time. A consequence of that will be the appreciable phase lag between $-\partial v_r/\partial r$ and f_r. Therefore, it is appropriate to use the reference frame of moving fluid (Lagrangian coordinates) to integrate Eq. (4).

Second, in a diwhirl core the maximal derivative $\partial v_r/\partial r$ is about $\pi v_{r,\max}/d \cong 1/(3\lambda')$. Therefore, the term $\lambda\dot{\epsilon}$ in (4) becomes of the order of unity and cannot be neglected now. Rewriting (4c) as $\lambda(d\tau_{rr}/dt) = -2\eta_p\dot{\epsilon} - \tau_{rr}(1-2\lambda\dot{\epsilon})$, we see that the equation is not symmetric with respect to the sign of $\dot{\epsilon}$. So, negative radial stress, τ_{rr}, corresponding to positive $\dot{\epsilon}$ should grow faster and reach higher absolute values than positive radial stress at negative $\dot{\epsilon}$ of the same amplitude.[27] Thus, the elastic force, f_r, directed inwards, which is generated by the large positive $\dot{\epsilon}$ at the beginning of the inflow (Figs. 1 and 10), should be larger than f_r directed outwards, which is generated by the large negative $\dot{\epsilon}$ at the end of the inflow (close to the inner cylinder). Therefore, the elastic force produced by the inflow is, an average, directed inwards and reinforces the inflow, while in the outflow the average f_r should be close to zero due to smallness of $\lambda\dot{\epsilon}$ there.

The flow structure of a diwhirl is rather complex[18,25] and

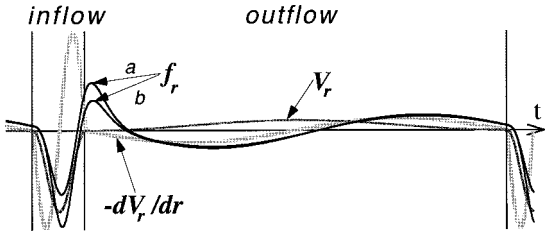

FIG. 11. Model velocity gradient, $-\partial v_r/\partial r$ (thick gray curve), and the elastic force, f_r (two thin black curves), experienced by a fluid element in a diwhirl flow as functions of time (in the Lagrangian coordinates). The first (**a**) curve $f_r(t)$ was calculated taking $\lambda\dot{\epsilon} \ll 1$, while for the second curve (**b**) was taken $\lambda a = 1/3$. The radial velocity, $v_r(t)$, is schematically shown by a thin gray line. $\partial v_r/\partial r$ is taken with the opposite sign in order to show the phase shift between $-\partial v_r/\partial r$ and f_r more clearly.

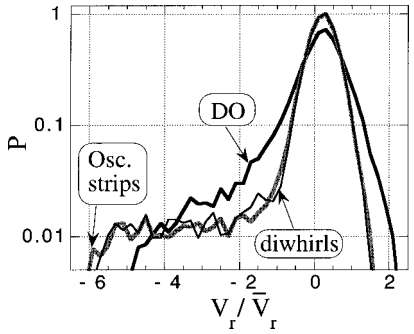

FIG. 12. Statistics of radial velocity, v_r, in DO (thick black curve), the oscillatory strips (gray curve) and the diwhirls (thin black curve). Probability density, P, is plotted in logarithmic scale against $v_r/\overline{v_r}$, where $\overline{v_r}$ is the rms of the distribution.

is not completely resolved at the moment. Hence, in order to evaluate the effect of the phase lag between $-\partial v_r/\partial r$ and f_r, we need to use some model dependence of $\dot{\epsilon}$ on time in the Lagrangian coordinates that would reflect the most important features of the diwhirl flow. One can infer from Fig. 10 that for both the inflow and the outflow such a model dependence can be one period of a sinusoidal $\dot{\epsilon}(t) = a \sin(\omega t)$. As the amplitude, a, of $\dot{\epsilon}(t)$ we take $\pi v_{r,\max}/d$, and as the frequency, ω, we use the expression $2\pi v_{r,\max}/d$, were $v_{r,\max}$ is the maximal radial velocity that is reached near the middle of the gap. Taking $v_{r,\max}$ in the inflow 8 times larger than in the outflow, as it is suggested by Fig. 9, and joining the two sinusoids together, we obtain the dependence of $-\partial v_r/\partial r$ on t in the Lagrangian coordinates, which is shown in Fig. 11. Since for the inflow $v_{r,\max}/d \cong 0.1/\lambda'$, we can take $\omega_{\text{in}}\lambda' = 1$ so that $\omega_{\text{out}}\lambda' = 1/8$, and the resulting $\dot{\epsilon}(t)$ has a period of $18\pi\lambda'$.

Substituting this $\dot{\epsilon}(t)$ into Eq. (4) and taking first $\lambda a \ll 1$, we obtain after integration the dependence of $f_r \equiv \Delta N_1/r$ on t that is shown in Fig. 11 by the thin black line **a**. Large velocity of the inflow produces significant phase lag between $-\partial v_r/\partial r$ and f_r, so that the elastic force is directed inwards during the major portion of the inflow and should be quite effective in driving it. On the other hand, in the slow outflow the phase lag between $-\partial v_r/\partial r$ and f_r is small and f_r averaged over the gap is directed outward, due to the initial overshoot produced by the inflow. As a result, the product $f_r v_r$ is positive, when averaged over the fluid element trajectory, so that the elastic forces make a positive work on the diwhirl flow.

This effect becomes even larger if a finite value of $\lambda\dot{\epsilon}$ is taken into account. The elastic force, f_r, obtained as a result of the integration of Eq. (4) with $\lambda a = 1/3$ is presented in Fig. 11 by the thin black line **b**. One can see that the narrow diwhirl core (the inflow region) is the region where $f_r v_r$ is large and where most of the energy is pumped into the diwhirl. In order to provide both the large phase lag between $-\partial v_r/\partial r$ and f_r ($\lambda(d\boldsymbol{\tau}/dt) \simeq \Delta\boldsymbol{\tau}$) and the strong radial elongation of the polymers ($\lambda\dot{\epsilon} \simeq 1$) the radial velocity in the diwhirl core has to be finite. Therefore, the diwhirls can only arise as a result of a discontinuous hysteretic transition, and $v_{r,\max}$ abruptly decreases to zero when the diwhirls decay.

The major asymmetry between inflow and outflow turned out to be a common property of the flow patterns presented in Fig. 6. This can be learned from Fig. 12, where the statistics of v_r for these three flow types are shown. The radial velocity was measured at constant r near the middle of the gap. The point of measurements was shifted along the column axis by steps of 0.5 mm and 25 measurements of v_r were taken in every point with an integration time of 0.1 s. For each flow pattern $1.5-2\times10^4$ velocity values were sampled. One can see in Fig. 12 that the statistics of v_r for the oscillatory strips [Fig. 6(b)] and for the diwhirls, that were gathered over ten strips and ten diwhirls, respectively, are almost identical. This distribution corresponds to the plot of $v_r(z)$ in Fig. 9. The statistics of v_r for DO share the same general features: a long tail at negative v_r and a maximum at $v_r > 0$. Therefore, the arguments presented above for the elastic forces driving the diwhirls can be applied to the oscillatory strips and DO as well.

IV. EXPERIMENT B

In the experiments reported in this section we explored CT flow of PAAm solutions with different polymer concentrations. We studied the dependence of the flow stability on the polymer contribution to viscosity, η_p/η. The experiments were carried out in a small CT column with $R_1 = 5.87$ mm, $R_2 = 7.37$ mm, and $L = 56$ mm at a constant temperature of 10 °C. The gap ratio, $d/R_1 = 0.255$, was close to the gap ratio in experiment A. The flow was visualized by the ambient illumination (2% of Kalliroscope was added to the solutions). Two series of experiments with different PAAm samples and Newtonian solvents were carried out.

In the first series we used the same PAAm sample as in experiment A. The Newtonian solvent was a 58% solution of saccharose in water. PAAm concentration, c, was varied from 23 to 500 ppm, which corresponded to η_p^0/η_s from 0.064 to 1.37. The solvent viscosity was $\eta_s = 0.0761$ Pa s. The polymer relaxation time, λ^0, was almost constant, slowly growing with c from 0.82 s at $c \to 0$ to 0.94 s at $c = 500$ ppm. So, the effects of polymer entanglement were tolerable in the studied region of concentration. The elasticity parameter, κ, changed from about 25 at $c = 23$ ppm, to about 65 at $c = 500$ ppm [because $\kappa \sim 1/t_{\text{vd}} = (\eta_s + \eta_p^0)/(\rho d^2)$].

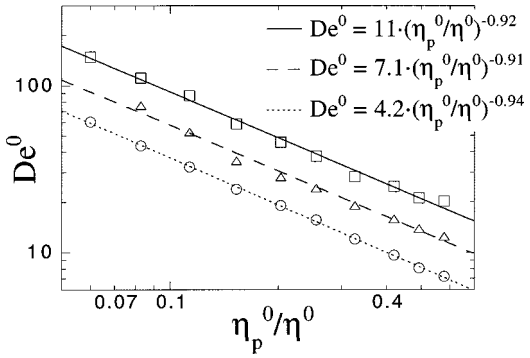

FIG. 13. Dependence of De^0 on η_p^0/η^0 at the onset of DO (squares), decay of DO to the oscillatory strips (triangles) and at the decay of the diwhirls (circles). The fits of the three dependencies to a power law $De^0 \sim (\eta_p^0/\eta^0)^{-\alpha}$ are shown by a continuous line, a dashed line and a dotted line, respectively.

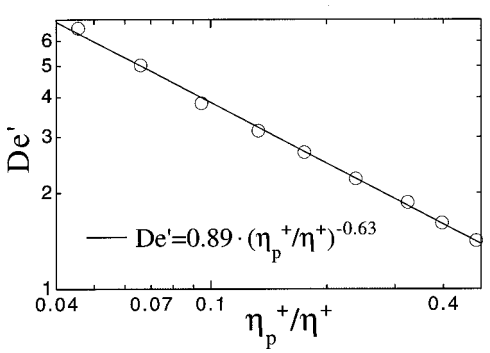

FIG. 14. Dependence of De' on η_p^+/η^+ at the diwhirl decay fitted by a power law.

In the whole studied region of c the sequence of flow patterns was found to be the same as in experiment A: Couette flow—RW-DO, as Ω was increased, and DO-oscillatory strips-diwhirls-Couette flow, if Ω was decreased afterwards. The Deborah numbers at different flow transitions are plotted in Fig. 13 as functions of η_p^0/η^0. The highest Reynolds number was less than 10% of Re_c, so that the inertial effects were always very small. One can see that the dependence of De^0 on η_p^0/η^0 for all the transitions can be well fitted by a power law $De^0 \sim (\eta_p^0/\eta^0)^{-\alpha}$, with the exponent α being about 0.92. This result is strikingly different from the prediction of LMS that implies $\alpha = 0.5$.

An obvious reason for this discrepancy is that the elastic dumbbell model and the Oldroyd-B equations that follow from it describe rheological properties of our polymer solutions only approximately.[1,2,4,14] The Oldroyd-B model implies that the polymer part of viscosity, η_p, the relaxation time, λ, and the first normal stress difference coefficient, Ψ_1, are constants. In contrast to it, our rheometric measurements showed that the shear thinning of η_p was as much as 60% at the largest shear rates and λ'/λ^0 at the same shear rates was as small as 0.1. (The shear thinning of Ψ_1 is discussed below.) The shear thinning is a function of the Deborah number (see Fig. 2). Since De at the elastic instability threshold is predicted to vary as $(\eta_p/\eta)^{-0.5}$, the effect of the shear thinning should be different at different η_p/η.

A straightforward way to correct the Oldroyd-B model for the shear thinning is to take shear thinned values of the relaxation time, λ', and of the polymer viscosity, η_p^+, for calculation of the Deborah number, $De' \equiv \lambda' \dot{\gamma}_{r\theta}$, and the polymer contribution to viscosity, η_p^+/η^+. Since both λ and η_p are decreasing functions of $\dot{\gamma}$ and De (see Fig. 15 for shear thinning of η_p), we expect the exponent α' in $De' \sim (\eta_p^+/\eta^+)^{-\alpha'}$ to be smaller than $\alpha = 0.92$ found for De^0 and η_p^0/η^0. The dependence of De' on η_p^+/η^+ at the diwhirl decay is shown in Fig. 14. Indeed, fitting it by a power law we obtain an exponent $\alpha' = 0.63 \pm 0.06$ that is rather close to the predicted exponent of 0.5.

This procedure of correction of the Oldroyd-B model prediction is not completely justified, however. According to LMS, the force driving the flow instability is due to the first normal stress difference and a proper generalized criterion of instability should be formulated in terms of N_1. The relation $N_1 \sim \lambda \eta_p \dot{\gamma}^2$ is specific for the Oldroyd-B model and may not hold for our polymer solutions at high De. In order to qualitatively verify the importance of N_1 for the development of the elastic instabilities, we used a 100 ppm solution of Xanthan gum in 58% saccharose in water ($\eta_p^0/\eta^0 = 0.61$) with relaxation time $\lambda^0 \simeq 1.5$ s at 10 °C. In contrast to PAAm, the molecules of the Xanthan gum are stiff, and their solutions exhibit very low N_1, while the relaxation time, λ, can be close to that of PAAm solutions. (The normal stress difference, N_1, measured in the Xanthan gum solution was about two orders of magnitude lower than N_1 in a PAAm solution with the same η_p^0/η_s^0 and λ^0 at the same shear rate.) Exploring the CT flow of the Xanthan gum solution we did not find any flow instabilities up to the highest reachable Deborah number, $De^0 = 600$. This result shows that the first normal stress difference and the hoop stress are indeed crucial for the observed flow instabilities.

Formulation of the instability criterion in terms of N_1 can be done as follows. Development of a flow perturbation is determined by balance between the driving force $\Delta N_1/r$ that is due to $\partial v_r/\partial r$, and the resisting force that is proportional to $\eta(\partial v_r/\partial r)/d$. For the Oldroyd-B model, ΔN_1 is proportional to $\lambda(\partial v/\partial r)N_1$, and we can suggest that this relation holds in a general case of a shear thinning polymer solution. Definition of the relaxation time, λ, for such a general case is not unambiguous, though. Indeed, in the above expression λ describes the extensibility of a polymer molecule by the secondary elongational flow in radial direction and it cannot be measured directly by the standard rheometry. We can suggest, however, that this relaxation time is proportional to $\lambda^*(\dot{\gamma}) = \Psi_1(\dot{\gamma})/(2\eta_p^+)$, which is, in fact, the common definition of relaxation time for the Boger fluids.[1,2] (In the above expression $\Psi_1(\dot{\gamma}) = -N_1/\dot{\gamma}^2$). Then the instability threshold will be determined by a nondimensional parameter

$$K^* = \frac{d}{2R_1}\frac{\lambda^* N_1}{\eta(\dot{\gamma})} = \frac{d}{R_1}\frac{\eta_p^+}{\eta^+}(\lambda^*\dot{\gamma})^2 = \frac{d}{R_1}\frac{\eta_p^+}{\eta^+}\,De^{*2}, \quad (6)$$

where $De^* \equiv \lambda^* \dot{\gamma}$. The instability should occur when K^* is raised above certain value. So, we recovered again the same form of the nondimensional control parameter as in Eq. (5), but now the Deborah number, De*, is explicitly defined via

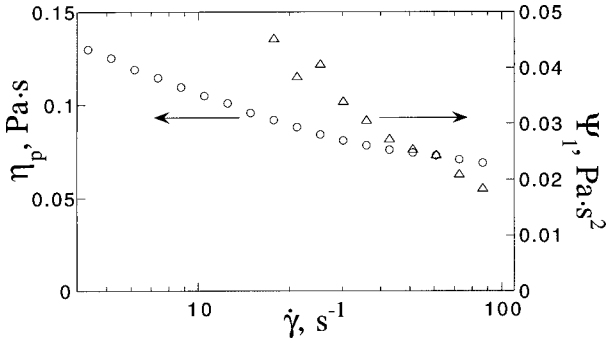

FIG. 15. Polymer part of the viscosity, $\eta_p(\dot{\gamma})$, and the first normal stress difference coefficient, Ψ_1, as functions of the shear rate, $\dot{\gamma}$, for a 600 ppm solution of PAAm (the first sample) in 58% saccharose in water at 10 °C.

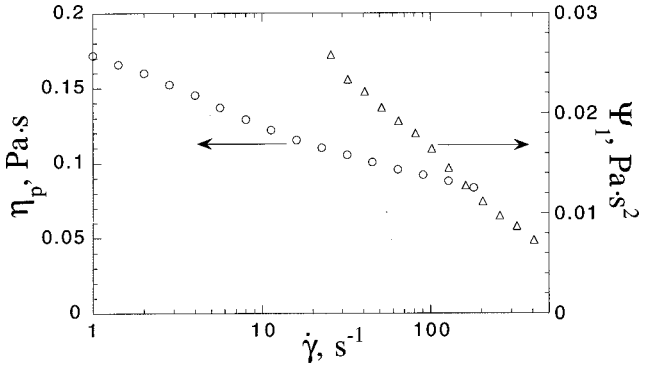

FIG. 17. Polymer part of the viscosity, $\eta_p(\dot{\gamma})$, and the first normal stress difference coefficient, Ψ_1, as functions of the shear rate, $\dot{\gamma}$, for a 500 ppm solution of PAAm (the second sample) in 63% saccharose in water at 10 °C.

N_1. Similar generalized instability criteria, though based on different arguments, were suggested previously.[14,17]

Verification of the instability criterion based on K^* requires accurate measurements of N_1 at the experimental shear rates. We have performed the measurements of the first normal stress difference with an AR-1000 rheometer of the TA Instruments. Measurements of N_1 in the PAAm solution used in the first series of experiments revealed significant shear thinning of $\Psi_1(\dot{\gamma})$ at the experimental shear rates. Typical dependencies of η_p and Ψ_1 on the shear rate, $\dot{\gamma}$, are shown in Fig. 15. Dependence of the generalized Deborah number, De*, at the DO onset on η_p^+/η^+ is shown in Fig. 16. One can see that this dependence can be well fitted by the power law $\mathrm{De}^* \sim (\eta_p^+/\eta_s^+)^{-\alpha^*}$, with the exponent $\alpha^* = 0.45 \pm 0.07$. This is very close to the exponent of 0.5 that follows from the relation $K^* = \text{const}$. The large uncertainty of α^* is mostly due to a systematic error that our data on N_1 at low c may be subjected to.

Unfortunately, resolution of the rheometer (about 2 Pa) was not sufficient for precise measurements of N_1 at the diwhirl decay in the whole experimental range. Thus, we had to use another PAAm sample with smaller molecular weight. Characteristic relaxation time of solutions of this second PAAm sample was about 6 times lower than λ of solutions of the first sample at the same η_s and η_p. Therefore, for the second sample, N_1 at the elastic instabilities in the CT flow was higher by about the same factor of 6, in agreement with the relation $\lambda^* N_1/\eta = \text{const}$.

In the second series of experiments we used solutions of the second PAAm sample in 63% of saccharose in water as a Newtonian solvent. The polymer concentrations, c, were 55–500 ppm, corresponding to η_p^0/η_s from 0.10 to 0.96. The solvent viscosity at the temperature of experiment (10 °C) was $\eta_s = 0.193$ Pa s. Typical dependencies of η_p and Ψ_1 on the shear rate, $\dot{\gamma}$, are shown in Fig. 17. One can see that both η_p and Ψ_1 decrease with the shear rate quite significantly.

The sequence of patterns in the CT flow was the same as in the first series of experiments (and as in experiment A) at all c. Dependencies of $\mathrm{De}^* = N_1/(2\eta_p^+\dot{\gamma})$ on η_p^+/η^+ at the onset of DO and at the decay of the diwhirls are plotted in Fig. 18. The values of the generalized Deborah number, De*, at the both flow transitions are quite close to those obtained in the first series of experiment with the first PAAm sample (Figs. 14 and 16). We notice, though, that De*, at the DO onset is about 30% lower that the Deborah number following from the prediction of Ref. 15. Both dependencies can be fitted rather well by $\mathrm{De}^* \sim (\eta_p^+/\eta^+)^{-\alpha^*}$ (Fig. 18). The exponent α^* was 0.50 ± 0.03 for the decay of the di-

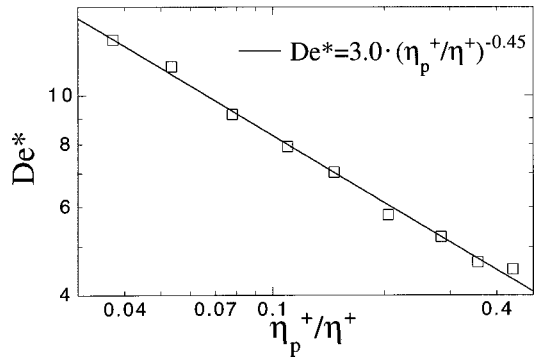

FIG. 16. The generalized Deborah number, $\mathrm{De}^* \equiv N_1/(2\eta_p^+\dot{\gamma})$, as a function of the shear thinned polymer contribution to the viscosity, η_p^+/η^+, at the onset of DO in the first series of experiments. The fit to a power law, $\mathrm{De}^* \sim (\eta_p^+/\eta^+)^{-\alpha^*}$, is shown by a continuous line.

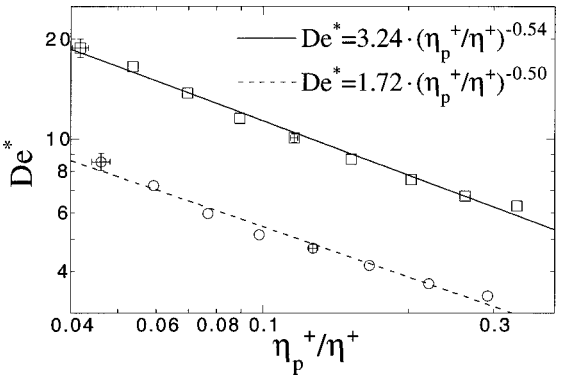

FIG. 18. The generalized Deborah number, De*, as a function of η_p^+/η^+ at the onset of DO (squares) and at the decay of the diwhirls (circles) in the second series of experiments. The fits of the two dependencies to a power law, $\mathrm{De}^* \sim (\eta_p^+/\eta^+)^{-\alpha^*}$, are shown by a continuous line and a dashed line, respectively.

whirls and 0.54 ± 0.03 for the onset of DO. The obtained values of α^* are very close to the expected value of 0.5.

V. DISCUSSION

The main goal of the experiments reported in this paper was to verify the applicability of the elastic instability mechanism suggested by LMS.[12] A specific feature of this mechanism is that the driving force, $f_r \equiv \Delta(\tau_{\theta\theta} - \tau_{rr})/r$, originates from coupling between perturbative radial elongational flow, $\partial v_r/\partial r$, and the strong azimuthal shear, $\dot{\gamma}_{r\theta}$. It was also supposed that for the driving force to be effective it has to be phase shifted with respect to $\partial v_r/\partial r$, and, thus, arising secondary flow should be oscillatory. The analysis in Ref. 12 was restricted to axisymmetric linear modes. Later, more accurate and extended calculations showed that the most unstable modes are always nonaxisymmetric[15] and elastic flow transitions occurring in the system are, probably, nonlinear.[24] Nevertheless, the basic suggestions of LMS concerning the origin of the driving force and the expression for the dimensionless control parameter, $K \equiv (\eta_p/\eta) \times (d/R_1)\mathrm{De}^2$, remained unchanged.

In our experiments we found that transition in the CT flow caused by the purely elastic instability is indeed strongly nonlinear. Therefore, we had to expand the original arguments of Ref. 12 to the situation where v_r is finite. From the simple discussion in Sec. II we concluded that action of the elastic force, f_r, is asymmetric with respect to inflow and outflow of finite amplitude. Thus, we suggested that flow patterns appearing as a result of nonlinear transitions should exhibit major asymmetry between inflow and outflow. This suggestion was completely validated by the velocity statistics of the diwhirls, oscillatory strips, and DO. Further, we showed that the elastic force, f_r, makes positive work in a flow of the diwhirl type, and, so, should be quite efficient in driving it. The phase shift between f_r and $\partial v_r/\partial r$ in this stationary flow is due to advection of the stress tensor that results in an effective oscillation frequency v_r/d. These results, we believe, are the most important evidence for the general validity of the instability mechanism suggested by LMS.

Further, constant De^0 at constant η_p^0/η^0 and d/R_1, and varying λ^0 that was found at the onset of DO and at the decay of the diwhirls in experiment A, is in full agreement with the prediction of LMS. The results of experiment B also agree with the theoretical prediction quite well, when the shear thinning effects are taken into account by reformulation of the instability criterion in terms of De* and η_p^+/η^+ [Eq. (6)]. The relation between De* and η_p^+/η^+ at the instability threshold that follows from $K^* = \text{const}$ is $\mathrm{De}^* \sim (\eta_p^+/\eta^+)^{-\alpha^*}$, with $\alpha^* = 0.5$, just as for an Oldroyd-B fluid. The exponents α^* found experimentally (Figs. 16 and 18) are in the range from 0.45 to 0.54, the deviations from the expected value of 0.5 being close to the uncertainties of evaluation of α^*.

Both experiment A and experiment B were designed to test the prediction of LMS that $K = \text{const}$ at the instability threshold and the results of both of them agreed with it. As it is shown below, however, the conditions of the two experiments are essentially different. That is why the predictions of the Oldroyd-B model were directly applicable for experiment A, while interpretation of the results of experiment B required correction for the shear thinning. On the other hand, the results of experiment A do not bear any specific information about the elastic instability mechanism, while the results of experiment B support the mechanism suggested by LMS.

Experiment A was carried out at constant c and varying temperature and η_s. In the whole experimental range η_p/η_s remained almost constant. As it follows from Fig. 3, for each temperature there existed characteristic time, λ^0, such that the response of the polymer stress, τ^p, to oscillations of the shear rate with amplitude $\dot{\gamma}_0$ and frequency ω was equivalent, if both $\lambda^0\dot{\gamma}_0$ and $\lambda^0\omega$ were kept the same. Further, the collapse of the dependencies of η_p/η_s on the shear rate at different temperatures (Fig. 2) onto a universal curve was obtained with the same relaxation time, λ^0, that resulted from the oscillatory tests. So, the shear thinning of η_p was a function of $\mathrm{De}^0 = \lambda^0\dot{\gamma}$ only. These results imply that the difference between the viscoelastic properties of the PAAm solution at different temperatures can be expressed by a single number—the value of the principal relaxation time, λ^0.[28]

Thus, the shear thinning of Ψ_1 should also be expressed by a universal function $g_1(\mathrm{De}^0) = \Psi_1(\dot{\gamma})/\Psi_1(0)$, where $\Psi_1(0)$ is defined as $N_1/\dot{\gamma}^2$ at $\dot{\gamma} \to 0$ and it should be proportional to $\eta_p^0\lambda^{0.2}$. Since shear thinning of all the fluid parameters depends only on De^0, the prediction of the constant Deborah number at instability threshold should not be influenced by the shear thinning. This can be seen, for example, from the generalized instability criterion, $K^* = \text{const}$, that at constant d/R_1 can be rewritten as

$$\frac{\lambda^* N_1}{\eta^+} = \frac{g_2(\mathrm{De}^0)\lambda^0 g_1(\mathrm{De}^0)\Psi_1(0)\dot{\gamma}^2}{g_3(\mathrm{De}^0, \eta_p^0/\eta^0)\eta^0} \sim \frac{g_1(\mathrm{De}^0)g_2(\mathrm{De}^0)}{g_3(\mathrm{De}^0, \eta_p^0/\eta^0)} \frac{\eta_p^0}{\eta^0} (\mathrm{De}^0)^2 = \text{const},$$

where we do not make any special suggestions about the form of the functions g_1, $g_2 = \eta^+/\eta^0$ and $g_3 = \lambda^*/\lambda^0$. Thus, the prediction of constant Deborah number at constant η_p/η and d/R_1 should hold not only for the Oldroyd-B fluids, but also for any polymer solution with the shear thinning that depends solely on De^0. This is exactly the case in experiment A.

As was mentioned above, the Deborah number defines the degree of stretching of the polymers by the primary shear flow and elastic stresses in the flow. Thus, constant De^0 at the flow transition thresholds actually does not point out to any specific instability mechanism. It is merely evidence that the observed transitions are driven by the elastic stresses.

For experiment B the flow transitions were predicted to occur at De varying as $(\eta_p/\eta)^{-0.5}$, so that the effect of the shear thinning was supposed to be different at different η_p/η. Therefore a correction for the shear thinning was absolutely necessary for comparison of the experimental results with the Oldroyd-B model predictions. Our generalization of the prediction of the Oldroyd-B for a shear thinning polymer solution was based on measurable shear thinning of Ψ_1. It

was rather straightforward and employed some suggestions about the connection between perturbations of N_1 and $\partial v_r/\partial r$ that were not verified directly. Nevertheless, the agreement between the dependence of De* on η_p^+/η^+ found experimentally and the relation $\mathrm{De}^* \sim (\eta_p^+/\eta^+)^{-0.5}$ following from $K^* = \text{const}$ was quite good. Such kind of relation between the Deborah number at flow transitions and the polymer contribution to viscosity is specifically connected to the structure of the Oldroyd-B equation and to the fact that the instability is normal stress driven. So, the results of experiment B can be considered as additional evidence for the validity of the mechanism of instability.

The connection between the perturbation of radial velocity, v_r, and changing of normal stress difference, N_1 is actually one of the crucial points of the instability mechanism. It is this connection that mainly defines the instability threshold. It cannot be obtained from the standard rheometric measurements performed in simple shear and elongational flows,[4] since the direction of the velocity perturbation is perpendicular to the main flow. Transitions from the Couette flow to DO and from the diwhirls to the Couette flow are both discontinuous. So, the problem of the pattern selection above the instability threshold involves behavior of the polymer solution in complex three-dimensional flows and is even more complicated.

Interpretation of the experimental results obviously requires some consistent rheological model. The drawbacks of the Oldroyd-B model are well revealed even in simple rheometric flows, because it does not take into account the shear thinning and finite extensibility of the polymers. The simple corrections for the shear thinning that we made worked well enough for the general functional dependence of the critical Deborah number on η_p/η. Nevertheless, the quantitative agreement between predicted De_c and the values of De* measured at the DO onset was rather poor. A few rheological models, like FENE and the Giesekus model,[4] have been developed to provide a more realistic description of the polymer solution rheology. These models incorporate the shear thinning and the finite extensibility,[4,14] and they have been recently used for treatment of the purely elastic instabilities.[14,17] Still, the models have not been extensively tested in complex three-dimensional flows. So, rheological properties of polymer solutions in the complex flows remain very much an open question that is also directly related to the turbulent drag reduction problem.[3,4] Further investigation of elastic instabilities combined with more elaborate and extensive rheometric measurements can be a good test of those rheological models. It can help us to better understand the behavior of polymeric fluids in complex flows.

ACKNOWLEDGMENTS

We would like to thank the anonymous referees for helpful comments. We are grateful to D. Bonn for his help with measurements of first normal stress difference. This work was partially supported by the Minerva Center for Nonlinear Physics of Complex Systems, by a research grant from the Philip M. Klutznick Fund for Research, and by the Israel Science Foundation Grant No. 92/96-1.

[1] R. G. Larson, ''Instabilities in viscoelastic flows,'' Rheol. Acta **31**, 213 (1992).
[2] E. S. G. Shaqfeh, ''Purely elastic instabilities in viscometric flows,'' Annu. Rev. Fluid Mech. **28**, 129 (1996).
[3] A. Gyr and H.-W. Bewersdorf, *Drag Reduction of Turbulent Flows by Additives* (Kluwer, London, 1995).
[4] R. B. Bird, Ch. Curtiss, R. C. Armstrong, and O. Hassager, *Dynamics of Polymeric Liquids* (Wiley, New York, 1987), Vols. 1, 2.
[5] R. H. Thomas and K. Walters, ''The stability of elasticoviscous flow between rotating cylinders. 2,'' J. Fluid Mech. **19**, 557 (1964); D. W. Beard, M. H. Davies, and K. Walters, ''The stability of elastico-viscous flow between rotating cylinders. 3. Overstability in viscous and Maxwell fluids,'' *ibid.* **24**, 321 (1966).
[6] R. F. Ginn and M. M. Denn, ''Rotational stability in viscoelastic liquids: Theory,'' AIChE. J. **15**, 450 (1969).
[7] B. J. A. Zeilinska, D. Mukamel, and V. Steinberg, ''Multicriticality in viscoelastic fluids heated from below,'' Phys. Rev. A **33**, 1454 (1986).
[8] H. W. Friebe, ''Das Stabilitätsverhalten verdünnter Lösungen sehr langkettiger Hochpolymerer in der Couette–Strömung,'' Rheol. Acta **15**, 329 (1976); R. Haas and K. Bühler, ''Einfluss nichtnewtonscher Stoffeigenschaften auf die Taylor-Wirbelströmung,'' *ibid.* **28**, 402 (1989).
[9] A. Groisman and V. Steinberg, ''Couette–Taylor flow in a dilute polymer solution,'' Phys. Rev. Lett. **77**, 1480 (1996).
[10] D. W. Bousfield, R. Keunings, G. Marrucci, and M. M. Denn, ''Nonlinear analysis of the surface tension driven breakup of viscoelastic filaments,'' J. Non-Newtonian Fluid Mech. **21**, 79 (1986).
[11] S. J. Muller, R. G. Larson, and E. S. G. Shaqfeh, ''A purely elastic transition in Taylor–Couette flow,'' Rheol. Acta **28**, 499 (1989).
[12] R. G. Larson, E. S. G. Shaqfeh, and S. J. Muller, ''A purely elastic instability in Taylor–Couette flow,'' J. Fluid Mech. **218**, 573 (1990).
[13] E. S. G. Shaqfeh, S. J. Muller, and R. G. Larson, ''The effect of gap width and dilute solution properties on the viscoelastic Taylor–Couette instability,'' J. Fluid Mech. **235**, 285 (1992); S. J. Muller, E. S. G. Shaqfeh, and R. G. Larson, ''Experimental studies of the onset of oscillatory instability in viscoelastic Taylor–Couette flow,'' J. Non-Newtonian Fluid Mech. **46**, 315 (1993); R. G. Larson, S. J. Muller, and E. S. G. Shaqfeh, ''The effect of fluid rheology on the elastic Taylor–Couette flow stability,'' *ibid.* **51**, 195 (1994).
[14] J. A. Byars, A. Öztekin, R. A. Brown, and G. H. McKinley, ''Spiral instabilities in the flow of highly elastic fluids between rotating parallel disks,'' J. Fluid Mech. **271**, 173 (1994); G. H. McKinley, A. Öztekin, J. A. Byars, and R. A. Brown, ''Self-similar spiral instabilities in elastic flows between a cone and a plate,'' *ibid.* **285**, 123 (1995).
[15] Y. L. Joo and E. S. G. Shaqfeh, ''The effects of inertia on the viscoelastic Dean and Taylor–Couette flow instabilities with application to coating flows,'' Phys. Fluids A **4**, 2415 (1992); ''Observations of purely elastic instabilities in the Taylor-Dean flow of a Boger fluid,'' J. Fluid Mech. **262**, 27 (1994).
[16] B. M. Baumert and S. J. Muller, ''Flow visualization of elastic Taylor–Couette instability in Boger fluids,'' Rheol. Acta **34**, 147 (1995); ''Flow regimes in model viscoelastic fluids in a circular Couette system with independently rotating cylinders,'' Phys. Fluids **9**, 556 (1997); B. M. Baumert, D. Liepmann, and S. J. Muller, ''Digital particle image velocimetry in flows with nearly closed path lines: The viscoelastic Taylor–Couette instability,'' J. Non-Newtonian Fluid Mech. **69**, 221 (1997).
[17] G. H. McKinley, P. Pakdel, and A. Oztekin, ''Rheological and geometric scaling of purely elastic flow instabilities,'' J. Non-Newtonian Fluid Mech. **67**, 19 (1996).
[18] A. Groisman and V. Steinberg, ''Solitary vortex pairs in viscoelastic Couette flow,'' Phys. Rev. Lett. **78**, 1460 (1997).
[19] K. Weissenberg, ''A continuum theory of rheological phenomena,'' Nature (London) **159**, 310 (1947).
[20] P. G. Drazin and H. Reid, *Hydrodynamic Stability* (Cambridge University Press, London, 1981).
[21] D. V. Boger, ''A highly elastic constant viscosity fluid,'' J. Non-Newtonian Fluid Mech. **3**, 87 (1977/78).
[22] We have slightly changed the original arguments given in pp. 591–593 of Ref. 12 by considering (for simplicity) time independent perturbation, $\dot{\epsilon}$.
[23] The original arguments in Ref. 12 were given for the case of very dilute solutions, when $\eta_p \ll \eta_s$ and, thus, $\eta \cong \eta_s$. Then the viscous resisting force is proportional to $\eta_s\, \partial^2 v_r/\partial r^2$, and the elastic instability threshold is defined by the value of expression $(\eta_p/\eta_s)(d/R_1)\mathrm{De}^2$. This result was confirmed by an accurate linear stability analysis.

[24]R. Sureshkumar, A. N. Beris, and M. Avgousti, ''Nonaxisymmetric subcritical bifurcations in viscoelastic Taylor-Couette flow,'' Proc. R. Soc. London, Ser. A **447**, 135 (1994).
[25]A. Groisman and V. Steinberg, ''Elastic versus inertial instability in a polymer solution flow,'' Europhys. Lett. **43** 165 (1998).
[26]M. J. MacDonald and S. J. Muller, ''Shear rheology of polymer solutions near the critical condition for elastic instability,'' Rheol. Acta **36**, 97 (1997).
[27]At $\lambda\dot{\epsilon}>1/2$, the growth of τ_{rr} should become unlimited that corresponds to infinite extension of the elastic dumbbells (Ref. 4), when the Oldroyd-B model is not adequate for description of the real finitely extensible polymers. It cannot occur here, however, since $\dot{\epsilon}$ is large only during short time intervals, $\Delta t \lesssim d/v_r \simeq \lambda$.
[28]Another parameter that changes with the temperature is the viscous diffusion time, $t_{\mathrm{vd}}=d^2\rho/\eta^0$. Effects of this changing of t_{vd} remain small, however, as long as $\mathrm{Re}=t_{\mathrm{vd}}\dot{\gamma}$ at the elastic instability thresholds is much less than Re_c (Ref. 25), Fig. 8.